# RESIDUAL STRESS ANALYSIS OF CERAMIC CUTTING TOOLS INDUSTRIAL APPLICATION

Tomohiro Shibata

Materials Science Department, Kennametal Inc.

1600 Technology Way, Latrobe, PA 15650 USA

Corresponding author: tomohiro.shibata@kennametal.com

## ABSTRACT

The residual stress states near the surface were analyzed for five commercially available ceramic metal-cutting tool inserts of compositions of β-SIALON, β-$Si_3N_4$, $SiC_W$ reinforced α-$Al_2O_3$, and two different carbides dispersed in α-$Al_2O_3$. From the standard side inclination stress measurement, a large deviation from a linear $\sin^2\psi$ dependence of lattice strain was observed near $\chi \sim 90°$ indicating a stress gradient along the depth direction near the surface. The information depth profiles of the lattice strain and the residual stress were obtained using a method similar to a thin film analysis. An exponentially decaying sinusoidal function was used to fit the *z* profile of the stress states for the samples studied. Information depth and *z* dependence of the residual stress states were evaluated, and the stress gradient was typically within 5-10μm from the surface, relaxed to the bulk region. For most of the inserts, stronger compressive residual stress was observed in the ground direction, whereas a weaker compressive stress or small residual stress appeared in the transverse direction near the surface. The final step grinding process seemed to be responsible for these differences. The capabilities and limitations in the application of the present analysis method to the metal cutting tool industries were discussed.

## INTRODUCTION

Ceramic metal-cutting tools have been used for wide varieties of applications including a high temperature machining of hard-to-cut materials because of their excellent high temperature material properties. Before being finalized as products, most of the ceramic tools go through various thermal and mechanical processes such as sintering, hot pressing, surface grinding etc. These processes may result in significant differences in residual stresses, which largely affect the tool performances. Compressive residual stresses are believed to be more beneficial for reducing a crack initiation and propagation, therefore final step grinding conditions must be chosen carefully in order to create desirable residual stresses in the machined surfaces (Brinksmeier and Wobker, 1989). For lightly ground ceramics, a very large stress gradient near the surface is frequently observed due to very confined heat affected zones mostly because of their poor thermal conductivities (Scholtes, 1987). For the research and development, and for quality controls, a practical but reliable depth profile characterization of the residual stress is beneficial

This document was presented at the Denver X-ray Conference (DXC) on Applications of X-ray Analysis.

Sponsored by the International Centre for Diffraction Data (ICDD).

This document is provided by ICDD in cooperation with the authors and presenters of the DXC for the express purpose of educating the scientific community.



Usage is restricted for the purposes of education and scientific research.

DXC Website
– www.dxcicdd.com

ICDD Website
- www.icdd.com

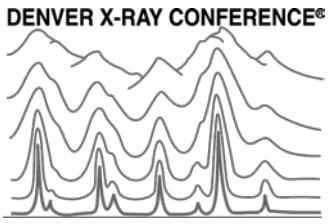


in tool industries; however, an analysis has rarely been conducted largely due to some technical difficulties including the limitation of resources. Stresses relax quickly away from the surfaces and determination using $\sin^2\psi$ dependence of strain (ε) may not be appropriate. We therefore applied the thin film stress analysis method to the characterization of ceramic surface regions using a laboratory x-ray diffractometer, and attempted to follow the method described for χ stress method herein (Birkholz and Genzel, 2006; Welzel *et al*., 2005). A residual stress with depth profile σ(z) will lead to a better understanding of the relation between the industrial process and surface residual stresses, and assist the research and development of tools with a better cutting performance. Our goal is a standardization of stress analysis in the industrial process and establishing in-house capabilities. We used metal-cutting inserts available in the market with different grades, geometries and different vendors in unused conditions. Particularly this time we picked samples found on our shelf, thus not necessarily having suitable size and shape for the academic studies.

## EXPERIMENTAL

### (a) Samples

Commercially available ceramics inserts with typical compositions (Whitney, 1994) were studied for different grades with (A) β-SIALON (B) β-$Si_3N_4$, (C) α-$Al_2O_3$ reinforced with SiC whiskers ($SiC_W$), (D) TiC dispersed α-$Al_2O_3$, and (E) TiMoCN dispersed α-$Al_2O_3$ composite ceramic inserts in unused conditions.

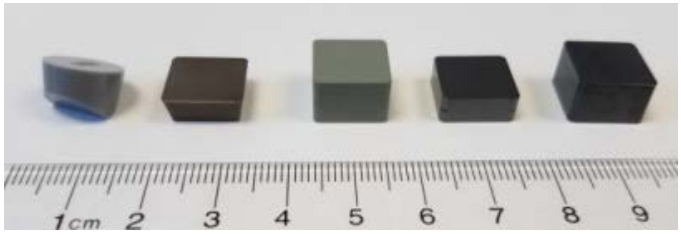


Figure 1: Samples studied. From left to right, (A) - (E). Top surface is rake surface, side surface is flank surface.

In Table 1, only major phases were listed determined by x-ray diffraction (PANalytical X'Pert MPD) and/or vendor provided literature. Since the details of the process were not disclosed, the ground direction and the transverse direction were conjectured based on the ground mark on the surface. The crystal orientations were relatively isotropic, which was concluded from a reasonable quality of Rietveld fit *without* including preferred orientations when measured with the Bragg Brentano geometry. Young's modulus (*E*), Poisson ratio (ν), and mass density (ρ) were measured with standard methods. The mass absorption coefficient for each phase $(\mu/\rho)_i$ was based on the crystal structure with observed lattice parameters, and the linear absorption coefficient of the sample $\mu^s$ was obtained as the sum of each phase $i$ as $\sum_i w_i(\mu/\rho)_i \rho$ with the weight fraction $w_i$, experimental ρ. These samples were chosen because of most common ceramics tool materials, with relatively small number of phase components. $E_{calc}$ is the average modulus of the composite calculated from those of each phase with $E_{calc} = \sum E_i v_i$ with $E_i$, and $v_i$, being theoretical $E$ and experimental *volume* fraction of the phase $i$ respectively (Richerson and Lee, 2006). From the physical properties, these ceramics, close to full densifications were realized.

Table 1: Samples used in the current study (the origin is not disclosed). C.S. denotes a crystal structure, H: hexagonal, C: cubic, R; rhombohedral. The PDF cards used for the phase analysis were also listed. The experimental Young's modulus (E), Poisson ratio ($\boldsymbol{\nu}$) was measured in house laboratory. Weight percent phase quantities were measured by XRD. $\tau_0$ is defined in the equation (1). --- denotes the phase not studied this time. The grain size of α-$Al_2O_3$ was not listed due to the blur edges, but the crystallites size is large and resolution limited of the diffractometer.

| Sample | Compositions | | | Physical properties | | | | | x-ray properties | | | | |
|---|---|---|---|---|---|---|---|---|---|---|---|---|---|
| | Phase | C.S | wt % | ρ ($g/cm^3$) | E (GPa) | ν | $E_{calc}$ (GPa) | Grain size (μm) | (μ/ρ) ($cm^2/g$) | $\mu^s$ (1/cm) | *hkl* | 2θ (°) | $\tau_0$ (μm) |
| A | β - SIALON 04-013-3345 | H | 92 | 3.15 | 290 | | | 0.5~3 | 38.3 | 122 | 301 | 51.8 | 16.1 |
| | $Al_5SiN_5O_2$ 04-021-4723 | H | ~ 8 | 3.37 | ---- | | | | 35.4 | | ---- | ---- | ---- |
| | Exp. | | | 3.20 | 228 | 0.28 | | | | | | | |
| B | β-$Si_3N_4$ 04-007-3040 | H | 100 | 3.20 | 310 | 0.27 | | 0.3~3 | 41.3 | 130 | 411 | 73.4 | 18.4 |
| | Exp. | | | 3.19 | 305 | 0.19 | | | | | | | |
| C | α-$Al_2O_3$ 04-003-5819 | R | ~85 | 3.95 | 380 | | | --- | 30.7 | 127 | 116 | 57.5 | 17.0 |
| | $SiC_W$ 04-010-5698 | H | ~15 | 3.21 | 460 | | | ~0.5× ~8 | 46.0 | | 110 | 60.2 | 16.6 |
| | Exp. | | | 3.77 | 400 | 0.18 | 389 | | | | | | |
| D | α-$Al_2O_3$ 04-003-5819 | R | 65 | 3.95 | 400 | | | --- | 30.7 | 326 | 116 | 57.5 | 6.4 |
| | TiC 04-007-5244 | C | 35 | 4.91 | 450 | | | 1~2 | 160 | | 311 | 72.5 | 7.2 |
| | Exp. | | | 4.29 | 424 | 0.22 | 420 | | | | | | |
| E | α-$Al_2O_3$ 04-003-5819 | R | 70 | 3.95 | 400 | | | --- | 30.7 | 292 | 116 | 57.5 | 7.1 |
| | TiMoCN 04-001-6529 | C | 15 | 6.95 | | | | 1~2 | 156 | | 311 | 72.5 | 8.1 |
| | $cZrO_2$ 98-004-1010 | C | 15 | 6.05 | | | | | 102 | | ---- | ---- | ---- |
| | Exp. | | | 4.85 | 411 | 0.21 | 421 | | | | | | |

## (b) Microstructure characterizations

The surface of the ceramic inserts were observed using a scanning electron microscope with the backscattering detector with two different magnification settings (2000× and 10000×) with the same acceleration voltage (15kV) shown in Fig.2. The surface was polished gently, minimizing the possible change the surface morphology, and then sputter-coated gold to obtain conductive surfaces. The ImageJ software (Schindelin *et al*, 2012) was used to enhance the contrast of the images for a better presentation. Sample (A) and (B) showed some elongated grains of ~10 μm from the hexagonal structure (A) β-SIALON, (B) β-$Si_3N_4$ phases, but majority of the crystallites were very small. Sample (C) showed whiskers grains of SiCw with very homogeneous size and aspect ratio with a preferred orientation. For (D) and (E), right angle edged grains were seen from the cubic TiC, or TiMoCN. For all α-$Al_2O_3$ containing samples (C)-(E), typical crystallites shapes as facetted triangular prisms, generally observed for separated ceramics grains, were not

observed. This might be because thin glass layers covered the grain surfaces during the sintering and cooling process. Indeed, nearly all the sintered ceramics and cermets in our industries generally do not result in good quality images.

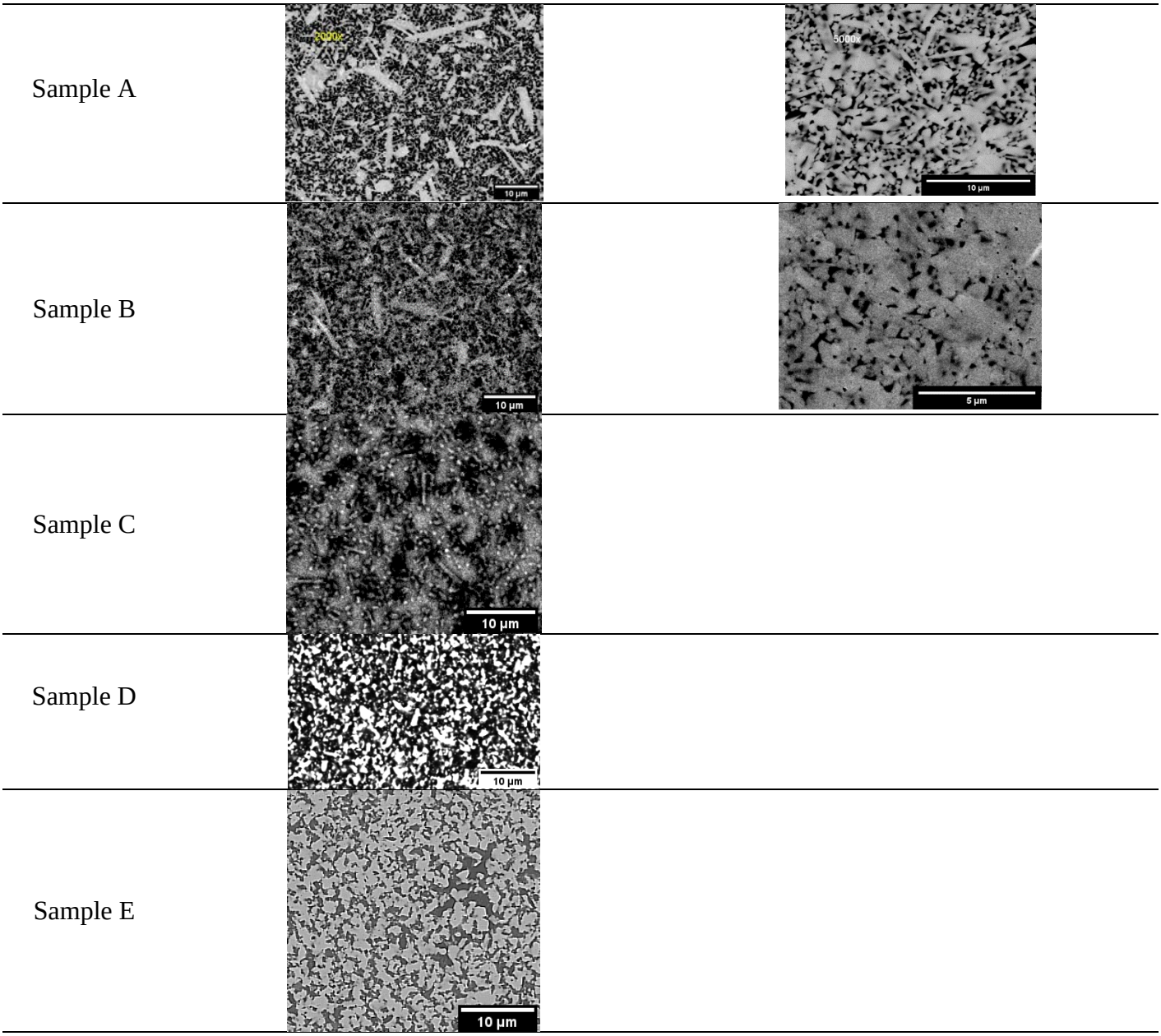


Figure 2: SEM images for samples (A) - (E). Left panel and right image were taken with 2000×, and 10000× respectively except for Sample (A) where the left panel is 2000×.

### (c) Residual stress experiments

The residual stresses were measured with a PANalytical X'Pert MRD diffractometer using a polycapillary lens at an incidence side, and a 0.18" parallel plate collimator and a proportional

detector at a diffraction arm. With a parallel x-ray geometry, de-focusing effect was negligible even at the angle close to $\chi$ = 90°. Cu K$\alpha_1$ radiation was used with the excitation of 45kV and 40mA. The x-ray beam slit size was typically chosen as 500×500μm ($w \times h$) with *w* and *h* being width and height of the slit size for the horizontal $\theta/2\theta$ goniometer configuration. The footprint on the sample surface is given as $(w/\sin\theta) \times (h\sqrt{1+(\tan\chi/\sin\theta)^2})$, thus a part of the x-ray beam was spilled from the samples surfaces at high angles $\chi \geq 82°$. The peak intensities were small at higher angles partly because of this. For the industry samples from the production, the surface area is not necessarily large enough and also squeezing down the x-ray beam size does not give reasonable statistics largely because of time limitations. However, the beam spill issues seem to be a minor effect on the peak positions; mainly reducing the intensities and raising the background levels with the help of soller slits and parallel beam collimators. Indeed the shift of the peak positions for the strain free tungsten (W) powders was less than 100 ppm with statistical variations for all the reflections, and less than 200 ppm for as-sintered ceramics samples (with smaller residual stresses) of the same size sample with the same geometry. Therefore the observed consistently large $\chi$ dependence of the peak shift for the present ground samples should be valid. Largely due to this, the intensity around $\chi \sim 90°$ was weak and 24 hours to 48 hours total were spent for most of the phase studied.

The PANalytical Highscore version 4.6, and Stress Plus version 2.0 were used for data analysis. In $\chi$ stress mode, the information depth ($\tau$) was evaluated by,

$$\tau = \sin\theta\cos\psi/(2\mu) \equiv \tau_0\cos\psi \qquad (1)$$

where μ is a linear absorption coefficient, $\chi = \psi$ in $\chi$ stress mode, $\tau_0$ is an information depth at $\psi$ =0. Here $\cos\psi$ dependence of $\tau$ gives the depth profile of ε around the surface at close to 90°. We typically measured 2° steps or smaller for $\chi > 80°$ and evenly spaced grid of $\sin^2\psi$ for $\chi$ <80°. Due to the multi-axial nature of the stress component, $\phi$ =0°, 45°, and 90° were evaluated where $\phi$ = 0° (ground direction), 90° (transverse direction), and 45° (diagonal direction). The *hkl* reflection plane was chosen at highest 2θ angle without interference with the other peaks, typically reflection peaks at 2θ ~ 50-70° were chosen. The peaks were fit with Pearson VII after K$\alpha_2$ stripping, Lorentz Polarization corrections. For most of the samples studied, the lineprofile of the diffraction peaks was much wider at angles $\chi \geq 87°$ giving an asymmetric peak shape with tails at higher $2\theta$ angles. The line broadening should be correlated with the stress gradient near the surfaces where $\tau$ was small, possibly resulted from the size reduction of coherently diffracting domains, and increase of planer stacking faults and lattice distortion (Noyan *et al*., 1985). When the tails of the peaks were significant, the line profile was fit with two peaks of narrow peak at lower 2θ and a much broader peak at higher 2θ angle. The main narrow peaks at lower 2θ peaks were analyzed. (The higher angle broader peak did not change the position with $\chi$.) The error bars shown in Fig.4-8 were from the curve fittings, evaluated from a standard method. The uncertainties from those of modulus, Poisson ratio, intergranular interaction, *hkl* dependence *etc*. were not included in the error bars, therefore the absolute values in $\sigma(\tau)$, $\sigma(z)$ may contain larger uncertainties. For clarity of the plot, error bars were not added to all the data points.

The $\sigma(\tau)$ was calculated from ε($\tau$) using $\sigma(\tau) = \varepsilon(\tau)/F(\psi)$ with the stress factor $F(\psi) = [1/2s_2\sin^2\psi + 2s_1]$ (Birkholz, 2006). For relatively isotropic case, $1/2s_2$ and $2s_1$ can be

replaced with $(1+\nu)/E$ and $-2\nu/E$ respectively. To obtain correct $E, \nu$ is generally difficult, since they depend on *hkl* directions, interaction with other phases, and the plastic deformation etc. Despite many factors affecting the accuracies from non-ideal experiments, *rough* but *practical* evaluations of the stress states of the products would be very important and beneficial for the industries. For simplicity, we used $E$ and $\nu$ from the literature values for the single phase. Experimentally available quantity σ(τ) is a convolution of σ(z) with an exponentially decaying function explicitly expressed as $\sigma(\tau) = \int_0^\infty \sigma(z) e^{-z/\tau}\, dz / \int_0^\infty e^{-z/\tau}\, dz$ with τ, therefore an explicit z dependence, σ(z), is obtained by an inverse Laplace transformation. However, the inverse transformation is an ill-conditioned problem and difficult to solve for arbitrary equations, or a numerical solution for noisy data does not produce a reliable solution. Usually accepted analytical method is assuming a relatively simple smooth trial function $\sigma(z)$ and the fit the data with $\sigma(\tau)$ with a few fit variables. In this study, we used a trial function of

$$\sigma(z) = \sigma_0\ (\cos\beta z + A \sin\beta z)\, e^{-\alpha z}\ , \qquad (2)$$

which Laplace transforms to

$$\sigma(\tau) = \sigma_0\{(\alpha + A\beta)\tau + 1\}/\{(\alpha\tau+1)^2 + (\beta\tau)^2\}\,. \quad (3)$$

The fit was performed to $\sigma(\tau)$ with $\sigma_0, A, \alpha,$ and β being fit variables. In some cases, we added an additional $A' \sin\beta' z\, e^{-\alpha' z}$ term to $\sigma(z)$ when the fit became better. In this way, $\sigma(z)$ was an analytical function of which the inverse-Laplace transform of fit function $\sigma(\tau)$. The trial function expresses a surface compressive/tensile stress, with underneath stress compensation regions, with stresses in oscillatory decaying with distance. Conventional analysis from the slope i.e. $\partial\varepsilon/\partial(\sin^2\psi) = (1+\nu)\sigma_{\parallel}(\tau_0)/E$ was also performed using Stress Plus, and compared with the surface regions. With these comparisons, we ascertain consistency of the data between the surface region and $\tau = \tau_0$ within accuracies.

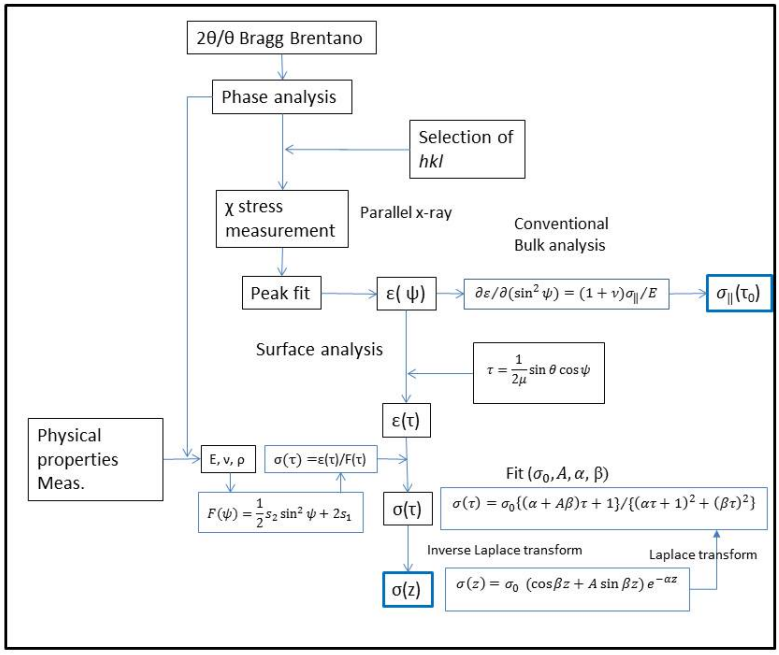


Figure 3: Residual stress analysis scheme.

## RESULTS

Information depth (τ) dependent residual stress, σ(τ), for Samples (A) - (E) are presented in Figure 4 - 8 respectively. First, let us take sample (A) β-SIALON as an example. β-SIALON has a hexagonal crystal structure similar as β-$Si_3N_4$, with partial replacement of Si with Al, and N with O. In many cases a sintering aid was added for an ease of liquid phase sintering. The sample (A) was a round insert, *i.e.* cylindrical shape with a round rake surface with curved flank surface shown in Figure 1. For the measurement of flank face, the x-ray beam size was ensured to be less than 1/4 of diameter of the sample. Three directions of $\phi$ (ground, transverse, and their bisecting direction) are shown in each figure.

Representative $d(\sin^2\psi)$ is shown in (a) in the entire region and (b) linear region ($\sin^2\psi < 0.9$). The $d(\sin^2\psi)$ deviated from the linear dependence significantly, indicating the strongly non-linear stress distribution (Klaus *et al.*, 2008). The $\sigma(\tau_0)$ was determined as $-125 \pm 18$MPa from the $\partial\varepsilon/\partial(\sin^2\psi)$ in (b) also shown as arrows at the right side of σ(τ) plots in (d), (e), and for Fig.5-8. The FWHM rapidly increased and at the same time the integrated intensity decreased where *d*-spacing steadily changed shown in (c). Since onset of the decrease of the integrated intensity is at lower angle than the x-ray beam spill ($\psi$~82°), this is not solely from the sample size/beam size effect, but coming from the sampling volume and possible texture effects as well.

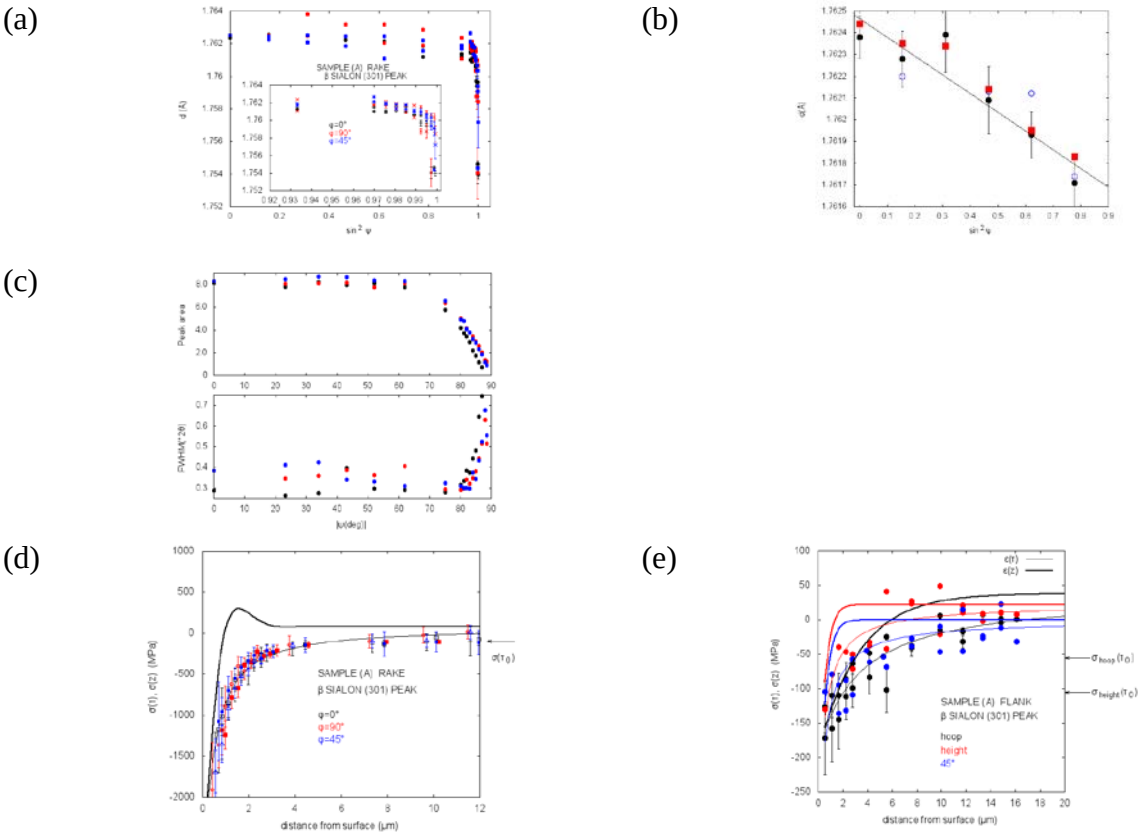


Figure 4 Sample (A) β-SIALON ceramic surface. Panel (a), (b) *d* spacing as a function of $\sin^2\psi$, (B) standard linear fit of the bulk residual stress. (c) Residual stress as a function of information depth. (d) full width at half maximum and peak area. Partial beam spill from sample surface for $|\psi| > 82°$, (e) residual stress of flank face. The thin line is a fit to the σ(τ), thick line is σ(z) for flank surface.

The data $\sigma(\tau)$ in the surface regions are fit with equation (3) with a few parameters and their inverse Laplace transform $\sigma(z)$ are shown with a *thin* line a *thick* line respectively for (d) rake (e) flank face. As seen in a literature by Huang and Predecki, (1997), $\sigma(z)$ appeared as a marked maxima near the surface, which was not obvious for $\sigma(\tau)$. In the current study, the data were fit with as described oscillatory decay model toward inside with reasonably well. The oscillation period was varied about the size of the grain size of the ceramic particles or type II residual stress, thus parameters giving unreasonably fast oscillation was avoided. For most of the ceramic surfaces, $\sigma(z)$ showed compressive stress near the surface region in the ground direction. The data were consistent with a stress relief region underneath, which decayed rapidly toward inside. The transverse direction for most of the samples showed much smaller compressive residual stress compared with the ground direction or very small residual stress states at very near the surface. The feature near the surface could be described with a sine term in equation (2). For all the ceramics, the strong $z$ gradient diminished below 5-10μm, i.e. within the depth of several grains, which would probably be because the heat affected depth or/and mechanically affected depth are limited. The different behavior between $\phi$ may indicate that the mechanical effect was still dominating in ground direction, whereas the mechanical effect is weaker and possibly comparable with the thermal effect in transverse direction.

As shown in Fig.4 (d), the $\sigma(\tau)$ of the rake face of sample (A) did not show significant $\phi-$ directional variations, which may certainly be attributed to the manufacturing process. The data were clean and steep stress gradient near the surface was observed. This may again be consistent with the shallow heat affected zone. No significant ground marks were seen on the curved flank surface, but a tendency of the compressive stress near the surface was still observed in $\sigma(\tau)$, indicating a small grinding effect. For sample (A) curved flank face (e), a poor counting statistics and small surface strain increased the uncertainty of the results. Possibly the discrepancies and discontinuity between $\sigma(\tau_0)$ and the extrapolated $\sigma(\tau_0)$ from $\sigma(\tau)$ was from the poor data quality for the flank surface.

Figure 5 shows the result of β-$Si_3N_4$. The sample was a positive angle insert, i.e. the angle between rake and flank surfaces is not a right angle. This made somewhat difficult for an alignment of the sample to the diffractomter for the flank surface measurement. For the rake surface, the ground direction showed a compressive stress below ~5μm, whereas the transverse and bisecting direction showed a weaker stress magnitude and gradient. For the flank surface, the ground direction showed a similar depth profile as the rake surface, but the transverse direction tended to be tensile stress near the surface. Both of the surfaces, and $\phi$ directions, the stress gradient was limited to 5μm from the surface. Despite the scatter of datapoints, the $\sigma(\tau)$ alone revealed a residual stress gradient, which would be a sufficient indication for research and quality assurance in the industrial processes in most of the cases. The stress state varied from two flank surfaces of the same insert shown in Figure 5(a) and (b). Stronger compressive stress was seen near the surface in bisecting direction in Face 2 seemed to be different from Face 1. Possibly subtle difference of grinding parameters might be sufficient to create a difference in the stress states.

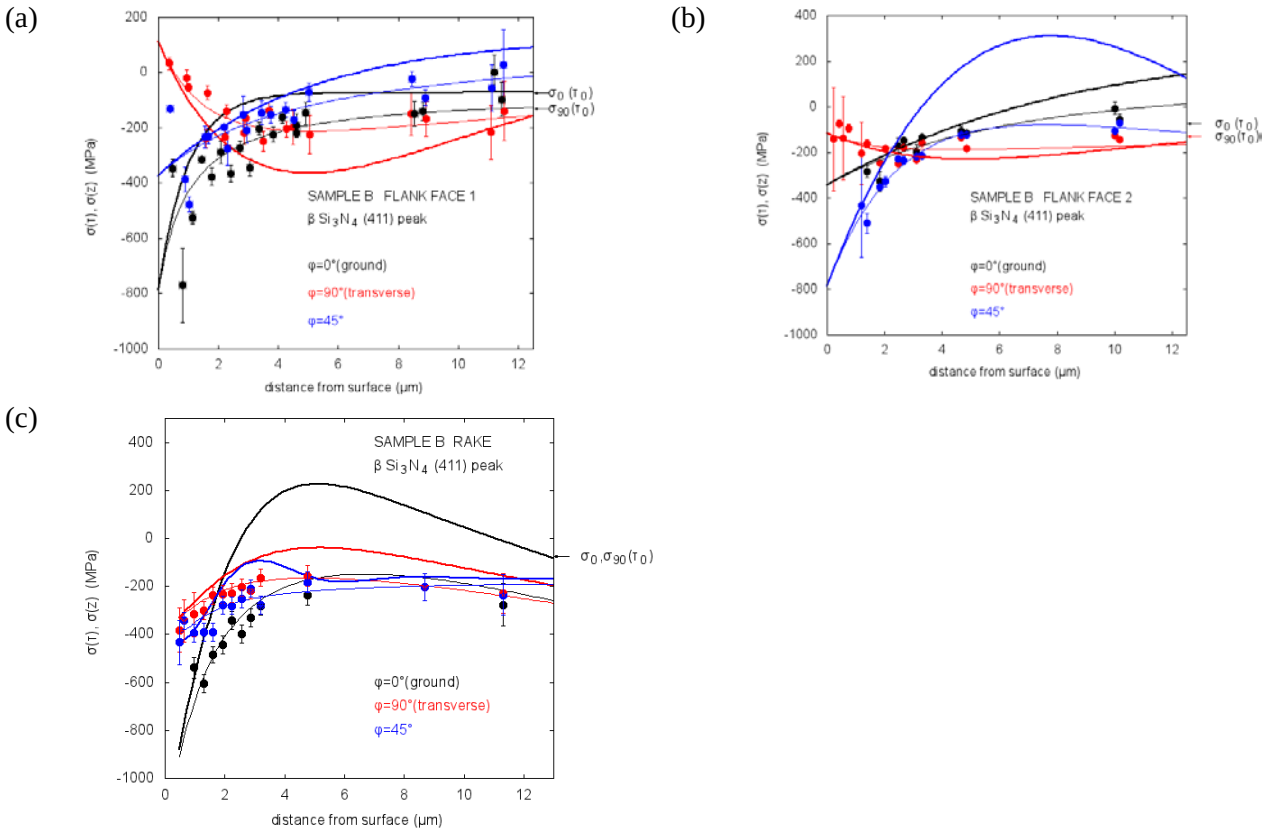


Figure 5: Residual stresses of sample B for β-$Si_3N_4$ phase. In addition to rake surface (c), two flank faces were measured for variations (a), (b). The thin line is a fit to the σ(τ), thick line is σ(z).

Figure 6 was the data for $SiC_W$ reinforced α-$Al_2O_3$. $SiC_W$ was often introduced in α-$Al_2O_3$ lattice for toughening mechanism. The α-$Al_2O_3$ (116) gave little point-to-point variations, and with fairly large compressive stress at the surface. Yet, in the transverse direction, the surface region showed a weaker compressive stress. The XRD spectra of $SiC_W$ was close to PDF01-089-2223, which is 39H (with Ramsdell notation), but highly possibly it was not a single polytype $SiC_W$. We used *hkl* peak with the high intensity and was separated from α-$Al_2O_3$ peaks, and without an asymmetric peak with turbostratic effect. The $SiC_W$ showed a weak stress gradient in σ(τ) around the surface. Because of the morphology of $SiC_W$, possible multiple phases, and anisotropies resulted in the extra scatter of the datapoints.

Figure 7 and Figure 8 were the α-$Al_2O_3$ based ceramics dispersed hard cubic carbides where α-$Al_2O_3$ and carbide phase were measured for the flank surface. Despite the different carbides, different phase, the residual stresses were consistently compressive in the ground direction, and the weak compressive stress or very small residual stress at around surface in the transverse direction. Generally the residual stress states is a result of the competing effects of mechanical (toward compressive) and thermal effect (toward tensile), the mechanical effect would be more dominant in the ground direction, whereas mechanical effect would be much weaker in the transverse direction, comparable to the thermal effects.

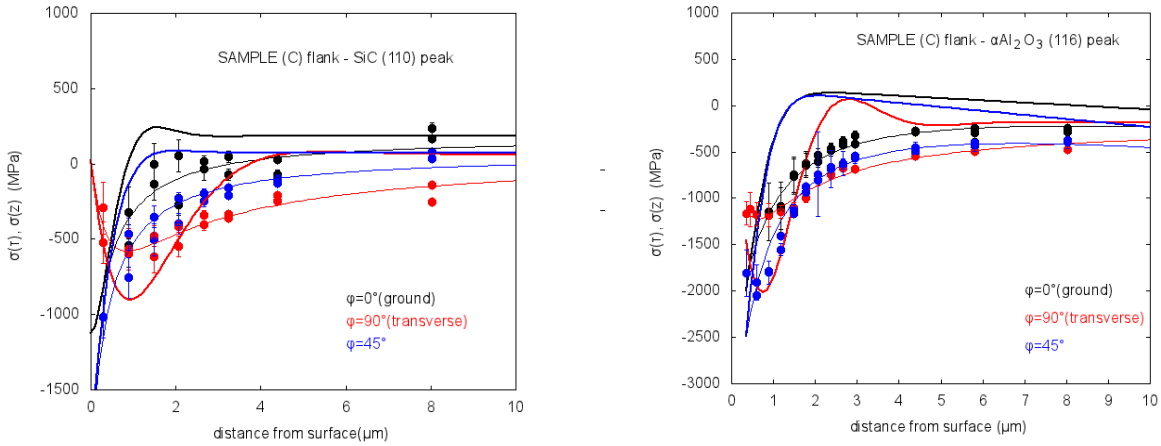


Figure 6: The residual stress for Sample C. $SiC_W$ and $\alpha$-$Al_2O_3$ phases were evaluated for flank surface. The thin line is a fit to the $\sigma(\tau)$, thick line is $\sigma(z)$

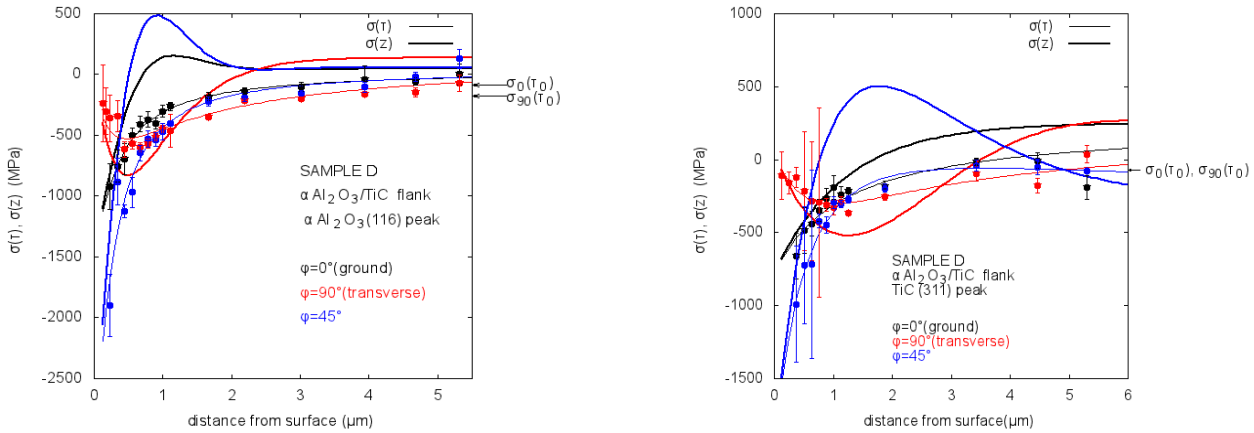


Figure 7: The residual stress for Sample D. TiC and $\alpha$-$Al_2O_3$ phases were evaluated for flank surface. The thin line is a fit to the $\sigma(\tau)$, thick line is $\sigma(z)$.

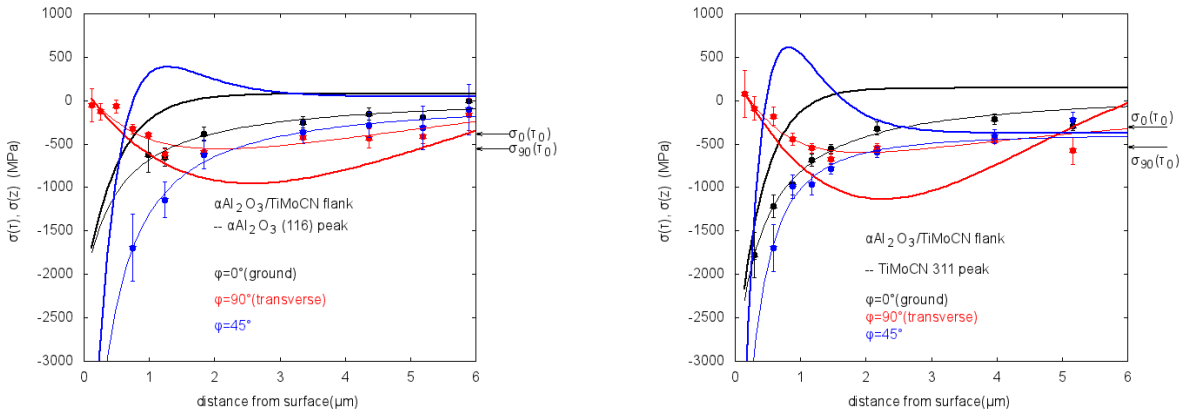


Figure 8 The residual stress for Sample E. TiMoCN and $\alpha$-$Al_2O_3$ phases were evaluated for flank face. The thin line is a fit to the $\sigma(\tau)$, thick line is $\sigma(z)$.

## DISCUSSION

From the $\psi$ dependence of the strain $\varepsilon(\psi)$ from the conventional $\chi$ stress measurement, $\varepsilon(\tau)$ was obtained in a relatively straightforward way by a simple geometrical consideration and some physical parameters. The stress factor $F(\psi)$ was used as a denominator at the conversion from $\varepsilon(\tau)$ to $\sigma(\tau)$ assuming relatively uniform textures; with the phase analysis prior to the stress analysis, weak texture was observed for most of the samples concluded from a reasonable Rietveld fit without a preferred orientation, thus this assumption would be reasonable. Uncertainties of Young's modulus and Poisson ratio from various sources such as the choice of reflection plane, interaction with the other phases/grains, and plastic deformation of the surface layers etc. impact the final values of the stresses. Further study will be needed to clarify correlations between morphologies of the grains consisting of the ceramics and residual stresses.

The observed strong $\psi$ dependence at close to 90° indicates the surface gradient of the residual stress of the ceramics. This should be due to the final grinding process, as expected from the directional grinding operations in $\phi$ plane. The other preceding processes were not expected to create directional dependence of the residual stress. For samples with multiple phases studied, the $\tau$ or z dependences of $\sigma$ were similar between each phase, which gave extra confidence about the results.

The observed stress depth profiles are rather complex, $\phi$ direction dependent, therefore the measurement of at least three different $\phi$ is desirable. Most of the analysis in the past avoided inverse Laplace transformation, and we followed their fashion. Instead of widely used $\sigma(z) = (a_0 + a_1 z + \cdots)e^{-z/z_0}$, and its transform $\sigma(\tau) = \frac{a_0}{\tau/z_0+1} + \frac{a_1\tau}{(\tau/z_0+1)^2} + \cdots$, we used exponentially damping sinusoidal function, which seems fairly versatile to express $\sigma(\tau)$. This can express the surface tensile stresses near the surface observed for transverse directions for several cases. Care was taken so that $\beta$ does not go too large compared with typical grain size, and x-ray resolutions.

Because of the scatter of the datapoints as well as the nature of the inverse Laplace transform, there still remains large ambiguity in the obtained $\sigma(z)$, not being uniquely determined. There have been many studies of depth resolved residual stress analysis using x-rays with different geometries such as $\chi$, $\Omega$, scattering vector (for example, Welzel *et al*., 2005). Among them, the side inclination method up to $\chi$ close to 90° seem to be a practical method for the metal-cutting industries, because it would be fairly insensitive against the non-ideal situations such as limitations of the sample size, sample flatness *etc*. Additionally the ease of the alignment of the samples may possibly reduce operator to operator variations. From the viewpoint of our industries, understanding the relationships between industrial processes and residual stresses, and further the relationship between the residual stresses and tool performance would be the next steps. Despite such an ambiguity in the residual stress, simply *information depth* profile $\sigma(\tau)$ or even $\varepsilon(\tau)$ would already be a sufficiently good indicator for further research in the industrial process used similar to "fingerprinting" methods.

## CONCLUSION

The residual stresses were characterized for five commercially available ceramic inserts of different compositions; α-SIALON, β-$Si_3N_4$, α-$Al_2O_3$/$SiC_W$, α-$Al_2O_3$/TiC, α-$Al_2O_3$/TiMoCN, with different geometries using χ stress measurement near χ ~90° for the surface region. All the samples show similar depth profile $\sigma(\tau)$ of the residual stress states near the surface. The observed depth profile of the residual stress was rather complex, and in most cases, the $z$ profile could be expressed with a sinusoidal function dumping toward the bulk region as $\sigma(z) = \sigma_0\ (\cos\beta z + A\sin\beta z)\, e^{-\alpha z}$. The surface stresses were confined typically within 10 μm range due to shallow affected zones of the grinding process. Ground directions showed a larger compressive stress, whereas the transverse direction showed a smaller compressive stress or tendency toward tensile in some case. Since the principle stress directions might not be either in the direction of ground or transverse, measurement of at least three angles $\phi$ =0°, 45°, and 90° is highly desirable. Despite some ambiguity of the process to deduce $\sigma(z)$, the characterization of $\sigma(\tau)$ or $\varepsilon(\tau)$ for the ceramic inserts should already be very beneficial for the research and development, and process controls, quality assurance in the productions in industries.

## ACKNOWLEDGMENT

The author acknowledges Kennametal team members, Loretta Bell, Kalissa Andre, Morris Ludwig, J. R. Ashbaugh, Joseph Tauber, Binky Sargent, Mark Garman, and Dr. Stefan Holzer for support of this project.

## REFERENCES

Birkholz, M. and Genzel, Ch., (**2006**). "Residual stress analysis" in *Thin film analysis by x-ray scattering*, *ed.* Birkholz.M. (Wiley-VCH, Weinheim) pp.239-295.

Brinksmeier, E. and Wobker, H.-G., (**1989**). "Residual stresses in tool ceramics and their influence on tool life" in *International Conference on Residual Stresses*, Beck, edited by G., Denis, S., Simon, A. (Springer, Dordrecht) pp. 267-272.

Eigenmann, B., Scholtes, B., and Macherauch, E., (**1989**). "X-ray residual stress determination in ceramics and ceramic metal composites", in *International Conference on Residual Stresses*, Beck, edited by G., Denis, S., Simon, A. (Springer, Dordrecht) pp. 27-38.

Huang, T.C., Predecki, P.K. (**1997**). "Grazing incidence x-ray technique for surface, interface, and thin-film analysis", Advances in X-ray analysis, 40.

Klaus, M., Genzel, Ch., Holzschuh, H., (**2008**). "Residual stress depth profiling in complex hard coating system by X-ray diffraction", Thin solid films, **517**, 1172-1176.

Le Bail, A., (**2009**). "The profile of a Bragg reflection for extracting intensities" in *Powder Diffraction Theory and Practice* ed. by Dinnebier, R.E. and Billinge, S.J.L., Cambridge UK, (RSC Publishing) p134-165.

Noyan, I.C., Cohen, J.B., (**1985**). "An X-ray Diffraction Study of the Residual Stress – Strain Distributions in the Shot-peened Two-phase Brass", Materials Science and Engineering, **75**, 179-193.

Richerson, D.W., and Lee, W.E (Eds) (**2006**). *Modern Ceramic Engineering, properties, processing, and use in design*" (Taylor & Francis. Boca Raton), 3rd. ed.

Scholtes, B, (**1987**). "Residual stresses introduced by machining" in *Advances in surface treatments in Technology-application-effects, vol. 4 International guidebook on residual stresses*, edited by Niku-Lari,A.,( Pergamon Press, Oxford).

Schindelin, J. *et al*. (**2012**). "Fiji: an open-source platform for biological-image analysis", *Nature methods* **9 (7)**: 676-682.

Whitney, E.D., (**1994**) (Ed) *Ceramic Cutting Tools* (Noyes Publications, New Jersey).

Welzel, U., *et al*., (**2005**), "Stress analysis of polycrystalline thin films and surface regions by x-ray diffraction", J. Appl. Cryst., **38**, 1-29.